PEG-in-PDMS drops stabilised by soft silicone skins as a model system for elastocapillary emulsions with explicit morphology control

Gaël Ginot, Martin Hamann, Leandro Jacomine, Friedrich Walzel, Antoine Egele, Damien Favier, François Schosseler, Mélanie Legros, Alain Carvalho, Catherine Foussat, et al.

Journal of Colloid and Interface Science 628 (2022) 1044–1057

Contents lists available at ScienceDirect

Journal of Colloid and Interface Science

journal homepage: www.elsevier.com/locate/jcis

PEG-in-PDMS drops stabilised by soft silicone skins as a model system for elastocapillary emulsions with explicit morphology control

Gaël Ginot, Martin Hamann, Leandro Jacomine, Friedrich Walzel, Antoine Egele, Damien Favier, François Schosseler, Mélanie Legros, Alain Carvalho, Catherine Foussat, Wiebke Drenckhan *

Institut Charles Sadrons, CNRS UPR22 - University of Strasbourg, 23 Rue du Loess, Strasbourg 67034 cedex 2, France

GRAPHICAL ABSTRACT

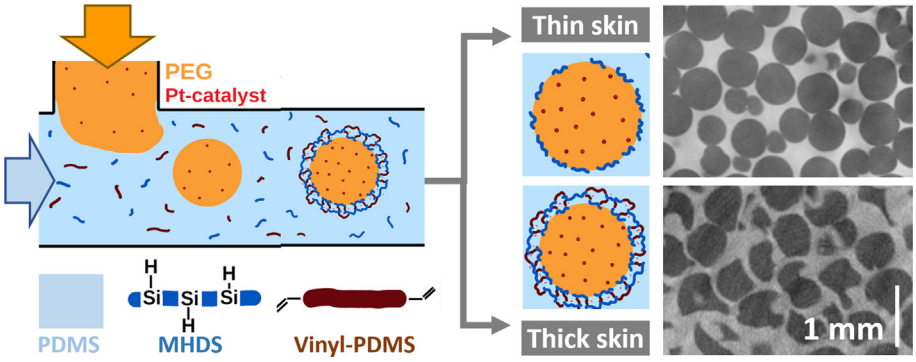

ARTICLE INFO

Article history:
Received 26 April 2022
Revised 1 July 2022
Accepted 4 July 2022
Available online 16 July 2022

Keywords:
Microcapsules
Elastocapillarity
Interfacial gel
Silicone
Emulsion
Interfacial rheology
Millifluidics
In-flow-chemistry

ABSTRACT

Hypothesis: The morphology of ordinary macro-emulsions is controlled by their high interfacial energies, i.e., by capillarity, leading to well-known structural features which can be tuned only over a narrow range. We claim here that a more explicit control over a much wider range of morphologies can be obtained by producing "elastocapillary emulsions" in which interfacial elasticity acts simultaneously with interfacial tension.

Experiments: We develop a model-system composed of PEG-in-PDMS emulsions, in which a catalyst diffuses from the PEG drops into the silicone matrix containing two reactive silicone polymers, which are cross-linked in a non-reactive silicone matrix to form a silicone gel of controlled thickness and mechanical properties on the drop surface. We characterise the cross-linking process of the gel in bulk and at the interface, and we analyse the skin growth kinetics. We then use the obtained understanding to produce emulsions with controlled elastocapillary interfaces using in-flow-chemistry in a purpose-designed millifluidic circuit.

Findings: We show that this approach allows to create interfaces over the full range of elastocapillary properties, and that very different emulsion morphologies can be generated depending on whether capillarity or elasticity dominates. These findings advance our fundamental understanding of the morphology of emulsions with complex interfaces, and they are of importance for the design of polymerised High Internal Phase Emulsions (polyHIPEs) with original structure/property relations. They will also be useful for the design of silicone capsules with fine-tuned mechanical properties.

* Corresponding author.
E-mail address: drenckhan@unistra.fr (W. Drenckhan).

https://doi.org/10.1016/j.jcis.2022.07.029
0021-9797/

1. Introduction

Many properties of foams and emulsions depend on their morphology, i.e. on how exactly the bubbles and drops are assembled in space. For foams/emulsions with macroscopic bubbles/drops ($> 10\ \mu m$), this morphology is essentially controlled by the minimisation of the energy associated with the liquid interfaces, which can be considered proportional to the interfacial tension γ and the interfacial area A [1]. Since the interfacial tension of most "ordinary" foams and emulsions with fluid-like interfaces can be considered constant, minimisation of interfacial energy is equivalent to the minimisation of the interfacial area under given constraints (constant bubble/drop volume). This leads to well-known topological and geometrical features of foam/emulsion morphology [1]. For example, in the limit of high dispersed volume fraction ($\phi_d > 90\%$), the structures follow Plateau's laws [2]: (1) Films separating neighbouring bubbles/drops have constant mean curvature. (2) Three films meet in a so-called "Plateau border" at angles of 120°. (3) Four Plateau borders meet in a vertex with tetrahedral symmetry.

These laws limit strongly the range of experimentally accessible foam/emulsion morphologies. This is of particular interest when liquid foams/emulsions are solidified for the generation of architected materials [3–6] with important consequences for their mechanical properties [7]. For example, one can show that Plateau's laws lead to materials dominated by bending deformations of the Plateau borders, rendering them inherently soft [7]. Controlled modification of Plateau's laws could lead to much stiffer materials and even materials with negative Poisson ratio [8–11]. With the rise of affordable 3D printing, any arbitrary structure can be generated with optimised structure/property relations [12]. However, this top-down approach reaches its limits for the generation of structures at scales close to or below its precision limit. Moreover, the production of large-scale structures with multiple length scales is inherently challenging for practical applications. These limitations encourage the investigation of bottom-up approaches, where original structures emerge from the mechanical self-assembly of the constituents of the material.

Moving away from morphologies controlled by the minimisation of surface area can be achieved by explicit modification of the interactions between the bubbles/drops in the liquid template. This can be realised by introducing friction and/or adhesion, or by rendering the interfacial tension dependent on deformation through solid-like interfacial elasticities. Fig. 1 shows an illustrative selection of examples from the literature. Systematic investigations into the relationship between complex interactions of soft grains and the resulting morphology have only started recently, being inspired by work on Pickering foams/emulsions [13], by the biophysics of cellular tissues [14–16] or by the physics of granular media [17–22]. A key challenge in these investigations is the access to experimental model systems whose bubble/drop interactions can be tuned explicitly and over a wide range.

In this article, we therefore develop an emulsion system with tunable solid-like interfacial elasticities. For this purpose, the interfaces of PEG-in-PDMS drops are covered with an elastic gel of cross-linked silicone polymers whose thickness and rigidity can be controlled separately. As sketched in Fig. 2a, these "skins" are created by dispersing catalyst-containing PEG drops of millimetric dimensions into a reactive silicone matrix composed of a non-reactive PDMS blended with two types of reactive silicone polymers undergoing hydrosilylation [32,33]. The progressive diffusion of the catalyst out of the PEG drops leads to the formation of a chemically cross-linked "silicone gel" on the drop surface. The properties of the skin can then be controlled explicitly via the formulation (Section 2.1) and the time which is left for the skin to grow.

The overall mechanical response of the drop surface is then controlled by the interfacial tension γ of the PEG/PDMS interface and by the elasticity of the silicone gel. The presence of both contributions turns the drops into "elastocapillary" objects akin to both a drop (interfacial tension only) and a balloon (solid-like interfacial elasticity only). We therefore refer to "droploons" in the remaining article. While interfacial tension tends to decrease the interfacial area of the two-phase system, interfacial elasticity tends to recover the reference shape of its zero-stress state. The interfacial elasticity therefore fundamentally alters the deformation response of the droploon when subjected to shape variations. As we showed in a

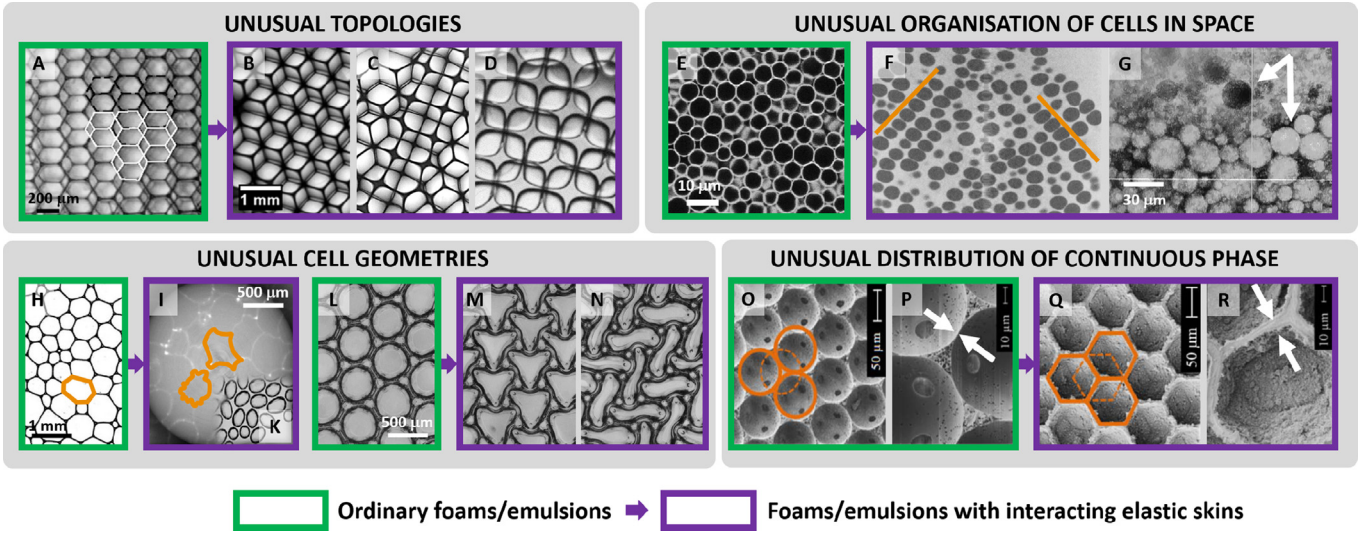

Fig. 1. Examples of "ordinary" foam/emulsion structures with liquid-like interfaces of constant interfacial tension (green frames), contrasted with unusual types of foam/emulsion structures (purple frames) which can be obtained by tuning the interactions between the bubbles/drops in the liquid template before/during solidification. A: Aqueous monodisperse foam with BCC structure from [23]. B-D: Crosslinked chitosan foams from [24] (B,C) and [25,26] (D) showing FCC (B) or SC structure (C,D). E: Slice through a standard emulsion structure from "Blair lab". F-G: PEG-in-Silicone emulsion with polymeric skins showing (F) organisation in force chains from [22] or (G) the possibility to mix PEG-in Silicone and Silicone-in-PEG emulsions [27]. H: Aqueous foam prepared using the detergent "Fairy". I: Buckled cell shapes of PEG-in-Silicone emulsion stabilised by polymeric skin from [27] K: Elliptical bubbles stabilised by silica nanoparticles from [28]. L/M/N: Crosslinking of hydrogel foams leading to mechanical constraints and buckling [29,30], O-R: Polystyrene foam made from a water-in-styrene HIPE using bulk-initiated polymerisation (O,P) or interface-initiated polymerisation (Q/R) from [31].

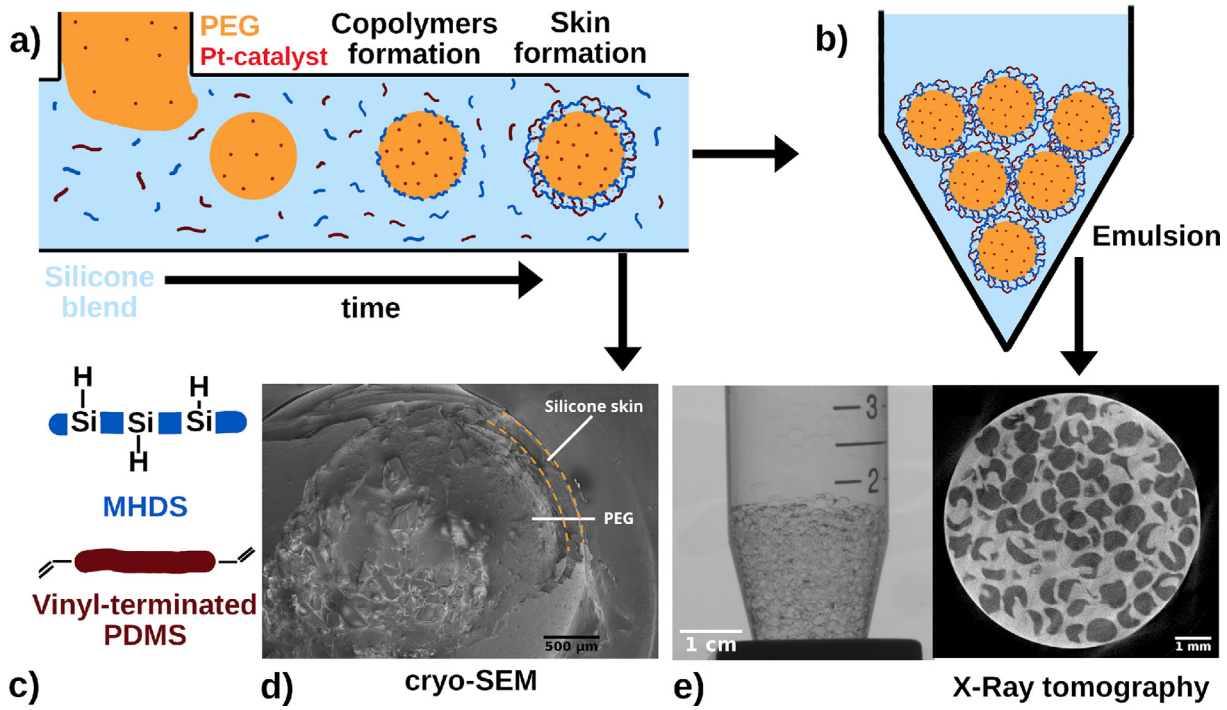

Fig. 2. (a) PEG drops containing a Pt-catalyst are produced in a reactive silicone blend with a millifluidic device. The skin formation is driven by the progressive diffusion of the catalyst from the PEG phase into the silicone phase. After the formation of copolymers at the interface, an elastic skin is formed by the crosslinking of the silicone blend (c) into a gel, turning the drop into a "droploon". This skin of controlled thickness and rigidity allows to tune the elasticity of the interface, stabilising unusual structures of emulsions created by collecting a large number of droploons (b). The droploons can be taken out of the sample to be imaged individually, e.g. with cryo-SEM (d), or be imaged directly in the sample with X-ray tomography (e).

previous paper [34], in the limit of an incompressible gel, its elasticity is fully characterised by its bulk shear modulus G and its thickness h_0. The competition between interfacial tension and elasticity can therefore be expressed by the elastocapillary number $\alpha = 3Gh_0/\gamma$. For small α, the system is dominated by surface tension, while for large α the system is dominated by elasticity. While emulsion morphology has been investigated in both of these limits [35,21,36,37], it is of particular interest to investigate intermediate α when surface tension and elasticity play on equal footing.

In Section 2.1, we describe in detail the formulations used throughout this article and the accompanying skin-forming reactions. In Section 3.1.1 we characterise the bulk properties of the silicone gels in absence of the PEG drops in order to obtain characteristic reaction time scales and some measure of the viscoelastic properties of the silicone gel. We then characterise the skin growth using interfacial rheology (Section 3.1.2) and X-ray tomography (Section 3.3). In Section 3.4 we translate the gained understanding of the gel formation at the interface into a millifluidic device designed specifically to produce large-scale samples of droploon emulsions. We put in evidence the difference in the associated emulsion structures, showing slices of these emulsions obtained with X-ray tomography and 3D analysis. In Section 4, we discuss the main conclusions and propose future improvements and potential applications of our system.

2. Materials and methods

2.1. Formulation

The molecular structures of all substances are presented in Fig. 3 and their main properties are summarised in Table 1.

The continuous phase of the formulation is a silicone blend which is composed of three different silicone polymers:

1. An unfunctionalised silicone oil ("PDMS", Fig. 3a) that is chemically inert under our experimental conditions;
2. A trimethylsiloxane-terminated methylhydrosiloxane-dimethylsiloxane copolymer with 25–35 % of all monomer units being methylhydrosiloxane units, which provide reactive Si-H groups ("MHDS", Fig. 3b),
3. A vinyl-terminated PDMS ("vinyl-PDMS", Fig. 3c).

The functionality of the vinyl-PDMS is $f_{vin} = 2$, while the functionality of the MHDS ($f_{MHDS} \approx 24$) was derived from its molecular weight and the manufacturer's specification that 25–35 % of the monomers of a MHDS molecule are methylhydrosiloxane units, i.e. reactive Si-H sites.

The stoichiometric ratio R of both reactive polymers is then given by

$$R = \frac{m_{MHDS}}{m_{vinylPDMS}} = \frac{M_{MHDS} f_{vinylPDMS}}{M_{vinylPDMS} f_{MHDS}} \approx \frac{5700\,\frac{\mathrm{g}}{\mathrm{mol}} \cdot 2}{7900\,\frac{\mathrm{g}}{\mathrm{mol}} \cdot 24} \approx \frac{1}{17}. \quad (1)$$

Since the Si-H groups of MHDS are located along the polymer chain creating steric hindrance (Fig. 3b) and since the initial Si-H group content might decrease during storage (sensitivity of Si-H groups to water or other active H-atoms) we use a slightly increased mass ratio of $R = 1/13$ for all reactive blends to ensure an excess of Si-H groups. We keep this ratio constant for all formulations.

We define the mass fraction ϕ_r of the reactive silicones as

$$\phi_r = \frac{m_{MHDS} + m_{vinylPDMS}}{m_{PDMS} + m_{MHDS} + m_{vinylPDMS}}. \quad (2)$$

To prepare the silicone blends, we mix all components with a magnetic stirrer for at least two days.

The second phase is a dispersion of a Platinum catalyst (platinum(0)-1,3-divinyl-1,1,3,3-tetramethyldisiloxane complex (0,1 M solution in vinyl-terminated polydimethylsiloxane, "Cat",

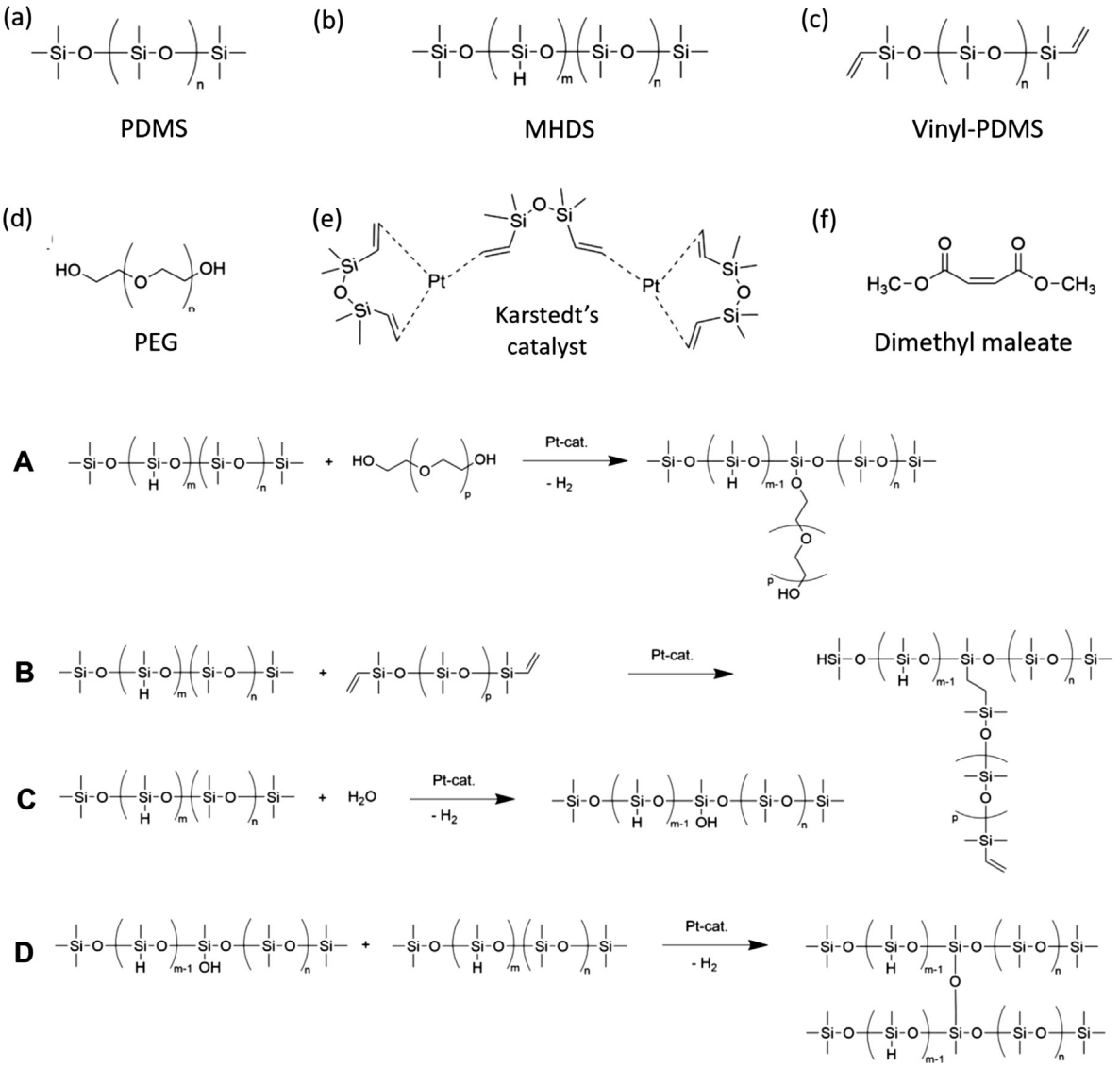

Fig. 3. (a)-(f) Different chemical components used in the formulation. The properties and full name of each component are listed in Table 1. (A)-(D) Different chemical reactions taking place in the system.

Table 1
Chemicals used in this article together with their main structural and physical properties.

Full name	Short name	Reference	Relative density (g/mL) (20 °C/25 °C)	Viscosity (cSt)	Molecular weight M_w (g/mol) [PDI] measured (provider)	Functionalisation degree f
Polydimethylsiloxane	PDMS	blackSIL FLD 47v100 (Elkem Silicones)	0.9674/0.9629	100	8800 [1.89] *(25000)*	0
(25–35% methylhydrosiloxane)-dimethylsiloxane copolymer, trimethylsiloxane terminated	MHDS	HMS-301 (Gelest Inc.)	0.9721/0.9674	25–35	5700 [1.91] *(1900–2000)*	≈ 24
Vinyl terminated polydimethylsiloxane	vinyl-PDMS	DMS-V21 (Gelest Inc.)	0.9682/0.9637	100	7900 [1.84] *(6000)*	2
Polyethyleneglycol 400	PEG-400	8.07485 (Sigma Aldrich)	1.126/1.122	97–110	*380–420*	-
Platinum(0)-1,3-divynil-1,1,3,3-tetramethyldisiloxane complex solution	Cat	479527 (Sigma Aldrich)	0.98 (provider)	NA	381.48	-
Dimethyl maleate		238198 (Sigma Aldrich)	1.152 (provider)	NA	144.13	-

Fig. 3e) in polyethylene glycol 400 from Sigma Aldrich ("PEG", Fig. 3d). Before making this choice we tested the purity of PEG-400 from three different providers (Section 1.2 in the Supplementary Information). To reduce side reactions with water (as discussed in Section 2.2), the PEG is dried at 40°C at 100 mbar for 16 h before each experiment (Section 1.2 in the Supplementary Information). The catalyst is dispersed in the dried PEG using an ULTRA-TURRAX disperser of 15 mm diameter at 6000 rpm for 2 min, before covering the solution under argon to avoid ambient water absorption. The quantity of catalyst added to the PEG phase is fixed by the volume fraction

$$\phi_{cat} = \frac{V_{cat}}{V_{cat} + V_{PEG}}, \tag{3}$$

where the choice of volume fraction (rather than mass fraction) was made because of the higher precision of measuring catalyst volumes with micro-pipettes.

To stop the skin-forming reactions, a dimethyl maleate inhibitor is added to the silicone blend ("Maleate", Fig. 3f). The phase composed of PDMS and dimethyl maleate inhibitor is prepared with a mass fraction of inhibitor

$$\phi_m = \frac{m_m}{m_m + m_{PDMS}}. \tag{4}$$

ϕ_m is chosen such that the molar ratio between the dimethyl maleate and the Karstedt's catalyst is 6:1 [38]. Both components are mixed with an ULTRA-TURRAX disperser of 15 mm diameter at 6000 rpm for 2 min shortly before use.

All chemicals are used as provided without further purification. The densities of the three silicone oils and the PEG are measured at 20°C and 25°C using the Excellence D4 densimeter from Mettler Toledo. The values for the viscosities are taken as given by the providers. The molecular weight of the three silicones was obtained via size exclusion chromatography ("SEC", see Section 1.1 in SI). We found these to be measurably different from the values given by the provider (see values in brackets in Table 1). For all our calculations we use the values from the SEC measurements.

2.2. Chemical reactions

The silicone skin is formed in two steps as schematically represented in Fig. 2a. The first step consists of a condensation reaction at the interface between the -OH end groups of the PEG and the Si-H groups of the MHDS (Fig. 3A) catalysed by the platinum-catalyst (Pt-cat). This reaction creates amphiphilic copolymers at the PEG-PDMS interface (Section 2.4) [39]. In a second step, the catalyst diffuses into the silicone phase enabling the formation of a cross-linked silicone gel which is formed by a (poly-) addition reaction between the Si-H groups of the MHDS and the vinyl groups of the vinyl-PDMS [32,33,40,41] as given in Fig. 3B. [42,38,43–45]. The functionalities of the vinyl-PDMS ($f_{vinyl-PDMS} = 2$), and the MHDS ($f_{MHDS} \approx 24$) lead to a highly cross-linked network.

The sensitivity of the Si-H groups to water creates a set of potential side reactions [46–48]. For instance, they may undergo a platinum-catalysed condensation forming a silanol group (Si-OH) while releasing hydrogen (Fig. 3C). This Si-OH group, in turn, may react with Si-H groups in a platinum catalysed condensation reaction to form a siloxane group (Fig. 3D). While silicone polymers are highly hydrophobic, the PEG is strongly hygroscopic, creating secondary reactions with water in the vicinity of the interface. As a consequence, drying of the PEG before use is necessary (Section 1.2 in the SI).

A model system for interfacial interactions in elastocapillary drops requires to stop the skin formation at the desired thickness h_0. Following the work of Lewis et al. [38], we opt for a dimethyl maleate inhibitor (Fig. 3f) which binds irreversibly to the Karstedt catalyst with a molar ratio 6:1, changing its structure and inhibiting its catalytic activity.

2.3. Bulk and interfacial shear rheology

Bulk and interfacial shear rheology measurements are performed with a TA Discovery HR-3 Hybrid Rheometer running under TRIOS 5.1.1.46572 software at 20 °C.

To control the onset of gelation for the bulk rheology we use a special preparation protocol for the samples. The silicone blend is divided into two separate mixtures: (1) MHDS blended with the unreactive PDMS, and (2) vinyl-PDMS blended with the unreactive PDMS and the platinum catalyst. Both parts are stirred for two days using a magnetic stirrer to ensure homogeneity of the blends. Before the experiment, 0.28 mL of the first blend and 3.60 mL of the second blend are put in two separate syringes (BD Plastipak 10 mL) which are connected via a luer connector, making sure that no air enters the system. The two liquids are then mixed by pushing back and forth on the pistons 30 times with roughly two pushes per second, before releasing the mixed blend onto the Peltier plate of the rheometer. The liquid is then injected between a stainless steel, sandblasted, parallel plate geometry at a gap distance of (1000 ± 1) μm. In order to avoid external constraints on the gel due to the shrinking/dilation of the blend during the gelation, the gap is continuously adjusted in all experiments in order to maintain a very small normal (compressive) force on the gel between 0–0.1 N.

During the experiment, the rheometer imposes an initial oscillating strain at 1% of angular deformation. We used the multi-wave frequency mode, allowing to probe the stress response at three frequencies simultaneously: 1 Hz (100% of the strain), 2 Hz (70% of the strain), and 4 Hz (50% of the strain). One data point is measured every 10 s. To avoid any slip or sample damage, the rheometer is programmed to reduce continuously the amplitude of the oscillations to maintain the measured torque values between 0.01 and 300 μNm. With this protocol we can measure a smooth increase of the elastic viscoelastic moduli with the advancement of the reaction until its completion.

Interfacial rheology is performed using a double-wall ring (DWR) geometry (patent No. 7,926,326) [49,50]. During the experiment, the rheometer imposes a 1% oscillating angular deformation at 1 Hz frequency. The two phases of the system (PEG phase: PEG + Cat, Silicone phase: PDMS + MHDS + vinyl-PDMS) are prepared separately as described in Section 2.1. For the experiment, the PEG phase is poured into the rheometer cup up to the groove of inner/outer diameter of 62.0/79.0 mm, respectively. The ring is positioned at the PEG surface. The silicone phase is then poured into the cup along its walls to allow for a slow, homogeneous deposition on top of the PEG phase until it reaches a height of 10 mm. One data point is measured every 10 s.

2.4. Surface tension measurement

The dynamic interfacial tension between the two phases is measured with the pendant drop technique using the TRACKER™ device from TECLIS®. A drop (10 μL) of the PEG-catalyst dispersion is formed in the reactive silicone blend (PDMS + MHDS + vinylPDMS) with a 1.63 mm wide needle. The interfacial tension is then monitored as a function of time through shape analysis of the drop in the regime where interfacial elasticity is negligible. The drop volume is maintained constant during the entire test via a PID control.

2.5. Skin growth characterisation on flat interfaces and individual drops

To obtain the temporal evolution of the skin thickness with controlled experimental parameters, we built a setup represented in Fig. 4I. It is made of a polycarbonate plastic block drilled with circular holes with a diameter of 5 mm. On top of the holes, we place metallic grids used in cryo-TEM, with square pores of 500 µm length, as shown in Fig. 4I. The block is then placed into a glass container, filled with the PEG-Cat mixture up to the top of the holes. The reactive silicone mixture is then slowly poured into the container, with a height of approximately 5 mm. In this configuration, the catalyst diffuses through the grid into the upper silicone phase, like in the double-wall ring setup (Section 3.1.1). After the desired reaction time, we remove the metallic grid from the silicone blend with the skin still attached to the grid. We leave the grid hanging vertically to remove the un-crosslinked silicone. The grid with the skin is then imaged using X-ray tomography (Section 2.7), with the height of the skin being taken as the height of the gel at the centre of a grid hole, as represented in Fig. 4II.

These measurements are complemented by Cryo-Scanning Electon Microscopy (CryoSEM) on individual drops. These are obtained by adding an individual PEG + catalyst drop into a vessel filled with the reactive silicone blend, and by rotating it continuously by hand to avoid prolonged contact with the walls of the vessel. After a given time the droploon is moved to a silicone blend with inhibitor to halt the skin formation. It is then placed on a grid so that unreacted silicone flows off the surface before freezing them in liquid nitrogen. The frozen skin is then broken with a thin metallic blade, before the drop is moved to the sample stage at -150°C of a Hitachi SU-8000 SEM at 1000 V acceleration voltage and a 9000 nA emission current.

2.6. Millifluidic setup

PEG in silicone emulsions are prepared using a millifluidic setup, represented in Fig. 4III. The reactive silicone fraction ϕ_r typically ranges between 50 wt.% and 100 wt.%, the catalyst fraction ϕ_{cat} between 0.1 vol.% and 1.0 vol.%, with a maleate mass fraction of ϕ_m of 5.5 wt.%. All the liquids are prepared following the procedure described in Section 2.1.

The reactive silicone phase is filled into two syringes (A) (60 mL PLASTIPAK), connected to a Y-junction with plastic tubes (TYGON E-3603) with an inner diameter of 1.59 mm. The two syringes are used with a double syringe pump (Harvard Apparatus Standard PHD Ultra) to impose identical flow rates leading to a total flow rate Q_{PDMS}. The PEG phase is filled into a single syringe (B) (60 mL PLASTIPAK), placed in a syringe pump (Harvard Apparatus Pump 11 Elite) and pushed at a flow rate Q_{PEG}. The two inlets are connected to a T-junction (C) of inner diameter 1 mm with plastic tubes (TYGON E-3603) of inner diameter 1.59 mm, with the PEG phase inlet plugged onto the perpendicular pipe of the T-junction. The size of the drops is controlled by the relative flow rates of the reactive silicone phase (Q_{PDMS}) and the PEG phase (Q_{PEG}). Typical flow rates for the stable production of monodisperse drops are: $Q_{PDMS} = 20$ mL/hr, $Q_{PEG} = 1.5$ mL/hr. Stabilisation of the drop production rate usually happens around 5 to 10 min after the beginning of drop formation. Drops produced before the stable flow are discarded and put directly in the waste container (H) at the end of the millifluidic setup. The outlet of the junction is plugged to a plastic tube (D) (TYGON E-3603) of inner diameter 2.38 mm. This tube, where the main reaction happens, is typically 40–240 cm long. It is coiled and kept flat and horizontal using a cross-shaped tube holder with drilled grooves of size matching the outer diameter of the tube.

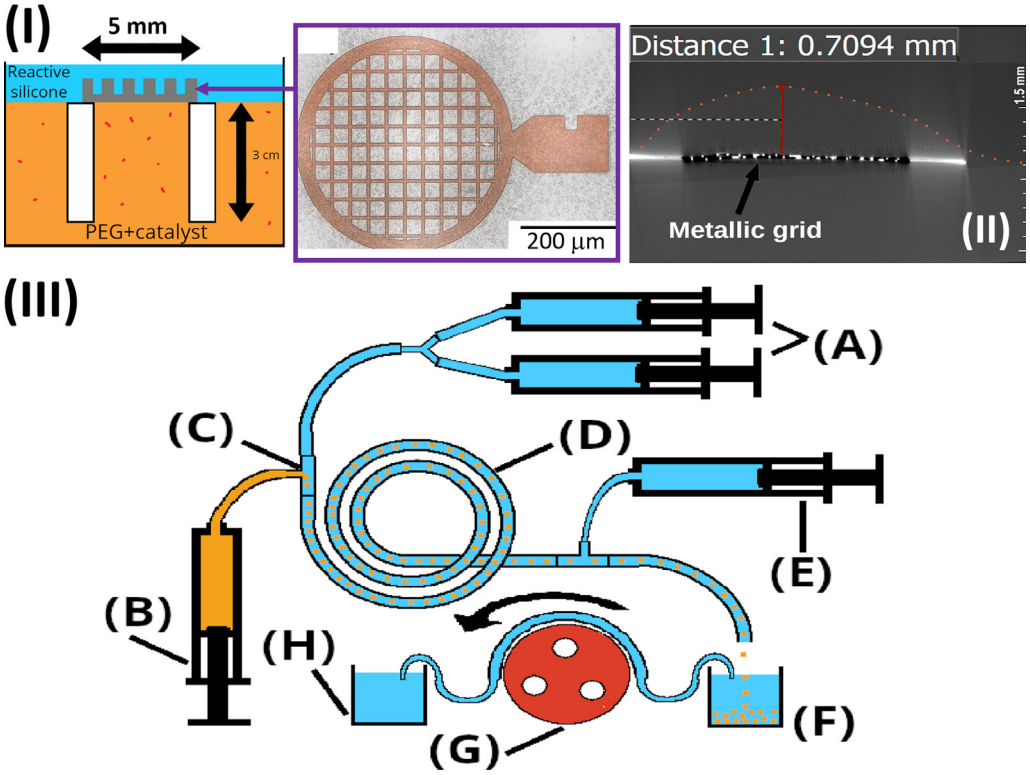

Fig. 4. (I) Setup to measure the skin growth kinetics by putting the reacting phases in contact through a grid which can be removed after a given reaction time and imaged by X-ray tomography. (II) Example of an image obtained with X-ray tomography. (III) Scheme of the millifluidic production setup. A: two syringes containing the reactive silicone phase (PDMS + MHDS + vinylPDMS). B: Syringe filled with the PEG phase (PEG + Cat). C: T-junction, where the drops are formed. D: spiral tube where the skin of the drop grows while being kept in motion by the laminar flow. E: syringe filled with PDMS and dimethyl maleate. F: sample container where the drops are collected. G: peristaltic pump removing the excess of silicone. H: silicone waste container.

This coiled tube (D) is the reaction chamber allowing skin growth. Its length allows to control the reaction time τ_r. Skins thick enough for detection with typical tomographic setup (10 μm) are obtained with reaction times of the order of 10 min, as shown in Section 2.5. In this time interval, the drops must be kept away from each other to avoid coalescence while the polymer skin forms. Additionally, long contacts with the walls of the tube are forbidden to avoid adhesion, which would lead to stretch and/or breaking of an inhomogeneous skin when collecting the drops.

At the end of the spiral tube (E), a PDMS blend containing dispersed dimethyl maleate is injected through a T-junction via a syringe pump (E) (60 mL PLASTIPAK pushed by Harvard Apparatus Pump 11 Elite) at a flow rate of 5 mL/hr. The exiting flow is then directed to a sample container (F) with a last plastic tube of 5 cm length. A camera takes photographs of the emulsion in front of a diffusive light source (Fig. 2e) for first visual inspection. Finally, as the silicone flow rate is large compared to the PEG one, the excess silicone in the emulsion needs to be removed. A peristaltic pump (G) (ISMATEC ISM832C) transfers the silicone into a waste container (H) when its volume reaches the top of the container.

2.7. Tomographic image acquisition

Tomographic projections of the emulsions are produced using the RXSolutions EasyTom setup. The X-ray source is a LaB6 filament in a Opentype Microfocus X-ray Source L10711 tube from Hamamatsu. It is calibrated using a black calibration (no X-ray emission) followed by a white calibration (no object between the detector and the source). The filament is powered with a DC current (90 kV, 60 µA) and follows the automatised warm-up procedure until it reaches a stable emission level. The filament is then set in large focal spot mode, limiting the generator power to 90 kV. The detector is a PaxScan 2520 amorphous silicon digital X-ray detector from Varian, with a 1920x1536 pixels matrix, each pixel with a 127 µm width. The projections are reconstructed into horizontal slices using XCAT filtered backprojection algorithm of the VGStudio software. Images are filtered using a noise reduction Butterworth apodization filter with 75% frequency. Borders are filtered to reduce projection overlap, using a vertical Tukey filter with 80% of the image area left unfiltered. We apply a ring filter on every slice with a 20 voxels kernel. We further apply a beam hardening correction with parameters automatically detected by XCAT. The final images have a resolution of 8x8x8 µm^3 per voxel.

3. Results

3.1. Characterisation of gelation kinetics and final gel properties

3.1.1. Bulk rheology

For reference purposes, we studied the bulk gelation of different reactive silicone formulations in the absence of PEG. After rapid blending of all components (Section 2.3), we followed the temporal evolution of the viscoelastic properties of the forming gel using a shear rheometre with the multiwave oscillation method ($\omega/2\pi$ = 1, 2 and 4 Hz). Fig. 5a,b shows a typical set of curves obtained for the evolution of the storage modulus G', the loss modulus G'' (Fig. 5a) and and the complex viscosity η^* (Fig. 5b) for one formulation (here $\phi_r = 30$ wt.% and $\phi_{cat} = 0.3$ vol.%). In these experiments, the evolution of the viscoelastic properties of the silicone matrix is that of a classic gelation: the silicone blend at the beginning of the experiment exhibits a liquid-like response, with $G'' > G'$. Over time, both increase, with G' increasing faster than G''. Eventually, G' becomes larger than G'' and the polymer blend becomes a gel. In the final stage, G' and G'' converge towards their final values G'_∞ and G''_∞, respectively. As expected, the characteristic values of the overall evolution depend on frequency.

In order to determine the gel time τ_g (time until the gel point is reached), the approach of Winter et al. [51,52] is commonly used. It relies on the fact that the tangent of the phase angle G'/G'' becomes independent of frequency at the gel point. However, this approach provided only very noisy data for our experiments. We therefore analyse instead the complex viscosity modulus η^* defined as $\eta^* = G''/\omega - iG'/\omega$. We define the gel time τ_g as the time of maximal variation of η^*, i.e when $d\log(|\eta^*|)/dt$ has a maximum. This is plotted in Fig. 5b for the example given in Fig. 5a. We find that this point is very well defined for all our experiments. As shown in Section 1.3 in the Supplementary Materials, we find that the variation of the final shear modulus G'_∞ and of the gel time τ_g with frequency is negligible within the investigated frequency range. This is why, in the following, we will only show the results of one frequency to simplify the graphs and the discussion.

In Fig. 5a-d, we show how G' and G'' vary for a wide range of formulations with different couples of reactive mass fraction ϕ_r (30, 50 and 70 wt.%) and catalyst concentration ϕ_{cat} (0.03, 0.1 and 0.3 vol%). Gels with the same ϕ_r have similar final moduli G'_∞, G''_∞. Increasing ϕ_r leads to stiffer gels. An increase in ϕ_{cat} has negligible impact on the mechanical properties of the gel, however, it decreases the gel time τ_g. The results for the gel time τ_g and the final storage modulus G'_∞ are summarised in Fig. 6a-d, which suggests that our data can be described satisfactorily by simple power laws

$$G'_\infty = A_1 \phi_r^{n_1}, \tag{5}$$

$$\tau_g = A_2 \phi_r^{n_2} \phi_{cat}^{n_3}, \tag{6}$$

where A_i and n_i are constants.

We use a statistical treatment, which is described in more details in the Supplementary Materials (Section 1.3) to check the reliability of Eqs. 5,6 and to obtain the values of the constants A_i and n_i. This treatment confirms the physically intuitive fact that the final storage modulus G'_∞ depends only on the reactive mass fraction ϕ_r, whilst the gel time depends on both, ϕ_r and ϕ_{cat}. Table 2 gives the final fit parameters obtained with the Levenberg–Marquardt algorithm [53] and the resulting mastercurves are plotted in Fig. 5e,f.

The exponent n_1 characterising the scaling of the storage modulus G'_∞ with the reactive mass fraction ϕ_r is surprisingly large. In the small deformation regime investigated here, basic arguments predict [54,55] that the elastic modulus of networks made from flexible polymer chains should be proportional to the density of effective elastic strands, the proportionality constant depending on the ability of the network junctions to fluctuate in space and on the topology of the network. Moreover the density of effective elastic strands is affected by the presence of defects like loops and dangling ends whose abundance depends on the concentration of the reactives [56]. In our case, due to the large size of the multifunctional units, the topology of the network is likely rather sensitive to the reactive fraction ϕ_r and this could explain the large n_1 value, reflecting simply the difference in network topology. The same caveat should apply for the exponent n_2 characterizing the gel time, which is highly dependent on the effective functionality of the junction points. Moreover the hydrosilylation rate is not constant and the relationship between conversion and time should depend on the concentration of reactives [40]. Finally, concerning the activity of the Pt catalyst, mechanistic studies have shown that it is rather complex [40] and depends on the amount of silane groups. Therefore, at this stage, Eqs. 5,6 should be considered merely as convenient empiric relationships used to tune separately the final gel elasticity and the gel time in the bulk silicone.

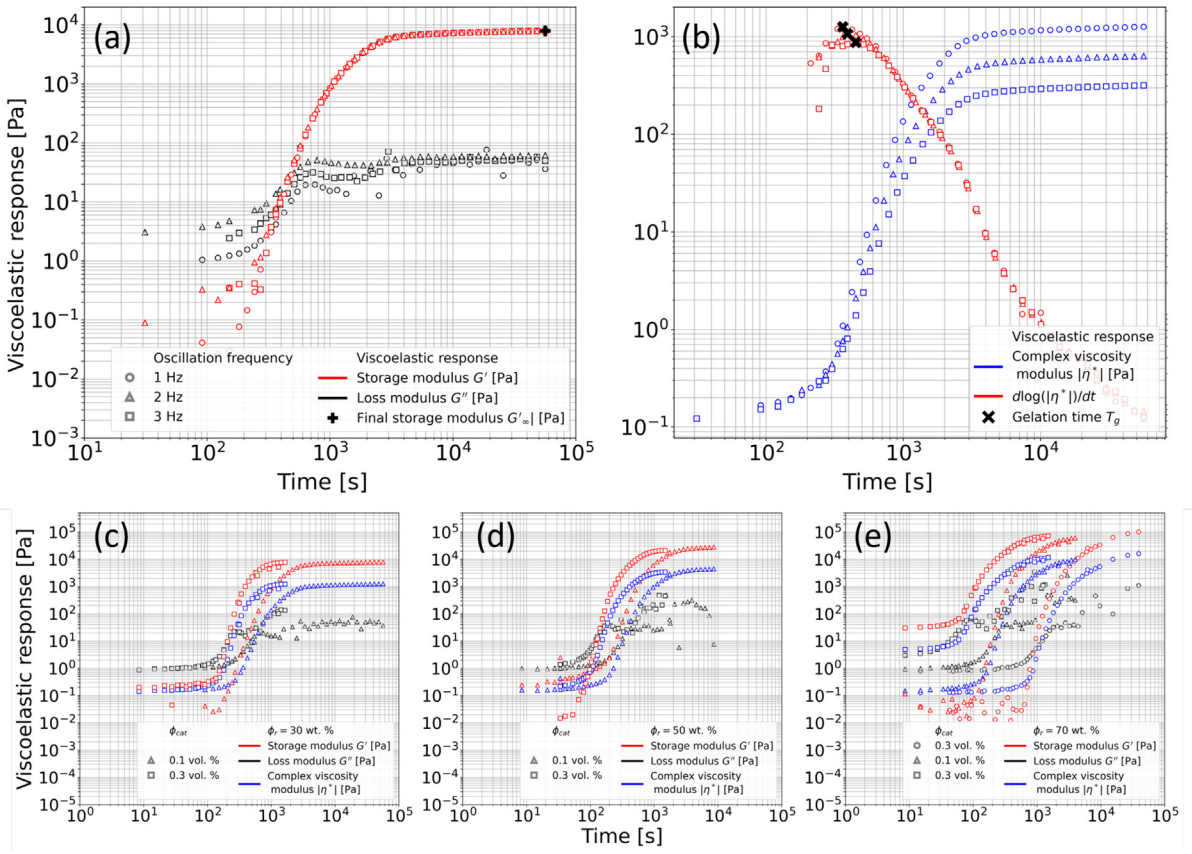

Fig. 5. (a) Example of the evolution of the viscoelastic response of the silicone matrix undergoing gelation with $\phi_r = 30$ wt.% and ϕ_{cat}=0.3 vol.% at oscillation frequencies of 1, 2 and 4 Hz. (b) The complex viscosity modulus is used to determine the gel time τ_g by taking the time at maximal slope for each frequency. The final storage modulus $G\prime_\infty$ is taken as the maximal value of the storage modulus G' over the whole experiment, for each frequency. (c)-(e) Temporal evolution of the viscoelastic response for different formulations varying the mass fraction ϕ_r of reactive polymers and the volume fraction ϕ_{cat} of the catalyst for an oscillation frequency of 1 Hz. (a) ϕ_r = 30 wt.% (b) ϕ_r = 50 wt.% and (c) ϕ_r = 70 wt.%.

If we make the assumption that the catalyst progresses by simple diffusion from the PEG drops into the silicone phase and that, to first order, the gel formation at the interface can be estimated similar to the one in the bulk studies, we can independently control the two key parameters of the elastocapillary number $\alpha = 3G'h_0/\gamma$, i.e., we can control the shear modulus G' through the reactive fraction ϕ_r and the gel thickness h_0 through the time allowed for the catalyst to diffuse through the interface before stopping the reaction. We can thus produce emulsions with different elastocapillary numbers and the same skin thickness h_0, or vice versa.

To test the inhibiting action of the maleate, we perform the same measurements in the presence of the inhibitor in the MHDS blend (Section 2.1). The results are shown in Section 1.4 in the Supplementary Materials. The storage and loss moduli remain constant over the whole experiment, indicating the lack of crosslinking in the silicone blend. For the millifluidic drop production (Section 3.4), we thus consider dimethyl maleate as an efficient inhibitor.

3.1.2. Interfacial rheology

The evolution of the shear rheological properties of the gel formed at the PEG/silicone interface upon diffusion of the catalyst from the PEG into the silicone phase is characterised with interfacial shear rheology (Section 2.3). The results for two reactive weight fractions ($\phi_r = 100$ wt% and 30 wt.%) at the same catalyst concentration ϕ_{cat} = 0.3 vol.% are shown in Fig. 7a.

The overall evolution of the mechanical response of the skin is similar to that of the bulk gel described in Section 3.1.1: an initially liquid-like system ($G\prime_{2D} < G''_{2D}$) becomes solid-like ($G\prime_{2D} > G''_{2D}$). These kind of observations are well known from the literature for rigidifying interfaces through absorption and/or crosslinking of interfacially active species [57,49,58–61]. We also observe that the evolution of the shear modulus of the interfacial gel differs from its bulk counterpart by the existence of two distinct regimes. A first regime, at short times, gives the interface a non-zero 2D shear storage modulus with characteristic values in the range of $G\prime_{2D} \approx 0.1$–1 mN/m. For both formulations, this first regime is very similar, the only difference being that it lasts longer for lower concentrations of reactive polymers (about 2000 s for $\phi_r = 100\%$ and about 4000 s for $\phi_r = 30\%$).

After a time of slow evolution at low values of $G\prime_{2D}$, the storage modulus increases by several orders of magnitude to values of the order of 1–10 N/m on timescales around 2.10^3 – 10^4 s depending on ϕ_r. The onset of this increase and the final value of $G\prime_{2D}$ depend on ϕ_r: the lower ϕ_r, the later the increase and the lower the final value of $G\prime_{2D}$. Interestingly, the increase in itself seems to produce initially the same slope in the logarithmic plot.

We explain the existence of the two regimes by the two different mechanisms at play in the skin formation (Section 2.2) as the catalyst diffuses through the interface. The first regime corresponds to the formation of PEG-PDMS copolymers at the interface created by the reaction between the PEG and the MHDS, as shown in Fig. 3A and schematised in Fig. 2a, and as already observed by Giustiniani et al. [39,62,22]. Confirmation of this interpretation is

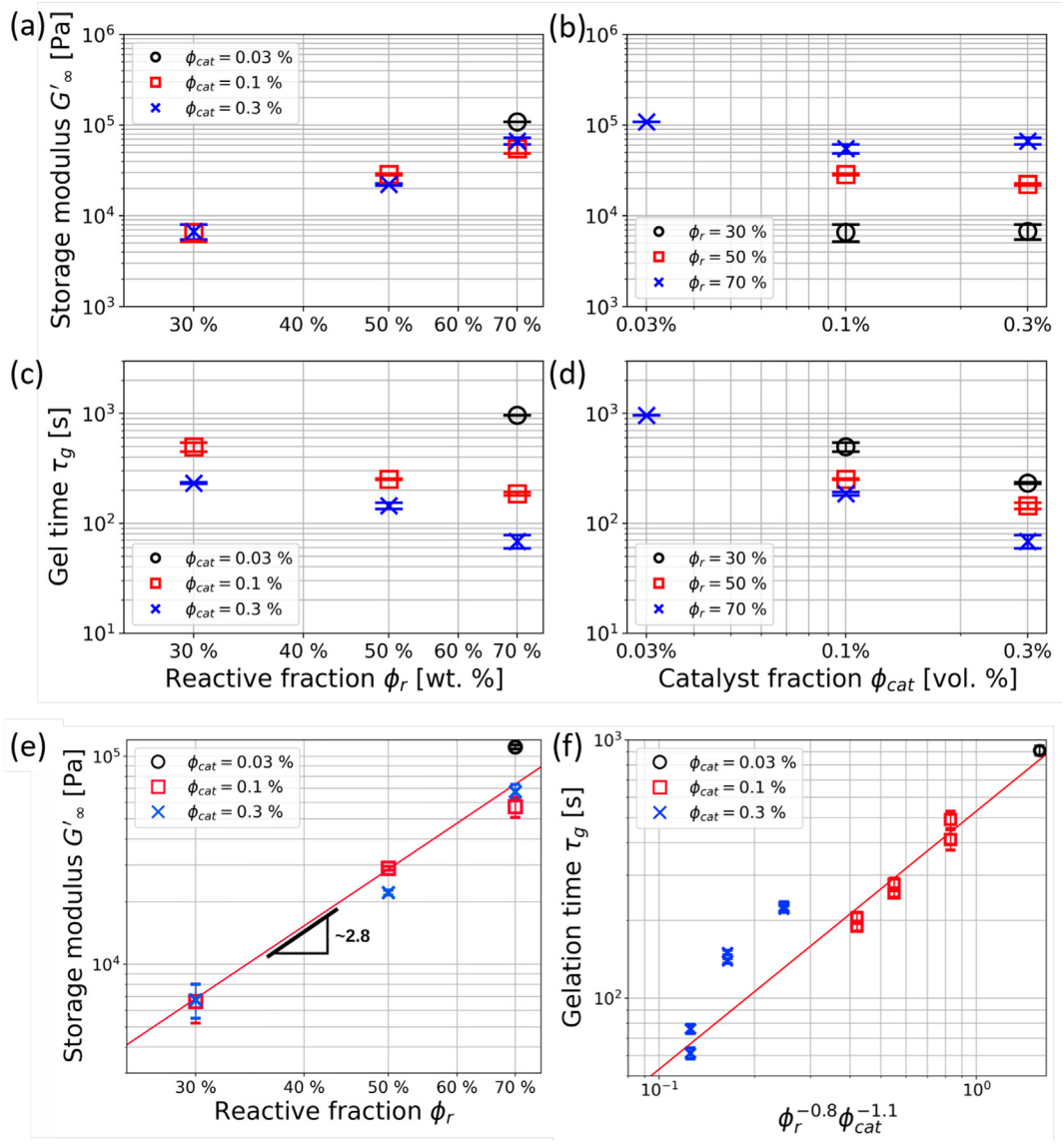

Fig. 6. Evolution of the final storage modulus G'_∞ (a,b) and the gel time τ_g (c,d) with reactive fraction ϕ_r (a,c) and catalyst fraction ϕ_{cat} (b,d). The results for the three frequencies are averaged, with their standard deviation shown as error bars. (e,f) Experimental data and scaling results obtained for (e) the evolution of the final bulk shear modulus G'_∞ with reactive fraction ϕ_r, and for (f) the evolution of the gel time τ_g with reactive fraction ϕ_r and catalyst volume fraction ϕ_{cat}.

Table 2
Values obtained by fitting the power laws given in Eqs. (5) and (6) to the data presented in Fig. 6.

A_1 (Pa)	n_1	A_2 (s)	n_2	n_3
0.49 ± 0.06	2.78 ± 0.01	616 ± 13	-0.80 ± 0.01	-1.09 ± 0.01

also obtained from the surface tension measurements discussed in Section 3.2. For the evolution of the shear properties of this layer, this step seems to depend little on the concentration of the reactive polymers ϕ_r, probably because the concentration in reactive silicone is not a limiting factor in the covering of the interface with the copolymer layer. The precise nature of the created layer/network still needs to be elucidated. It shall be noted that because of the importance of the catalyst diffusion kinetics towards the interface, this step is highly sensitive to the preparation of the PEG/catalyst dispersion described in Section 2.1.

In the second regime, the diffusion of the catalyst into the silicone phase starts to cross-link the reactive silicone polymers, forming the actual silicone skin. With increasing ϕ_r, the kinetics of this mechanism accelerates and the final shear modulus increases, similarly to the bulk silicone gel studied in Section 3.1.1. This gelation mechanism, however, differs from its bulk counterpart by its temporal aspect: the catalyst is initially absent from the silicone phase, into which it diffuses after the formation of the PEG-PDMS copolymers. The gelation kinetics is thus locally dependent on the concentration of catalyst, which itself depends on the diffusion timescale of the catalyst molecule. The advancement of the gelation front (i.e. the maximal thickness where the gel time τ_g has been reached) is thus dependent on the diffusion of the catalyst, and hence on its initial concentration. Moreover, the gelation continues to progress behind the gelation front, as the gel continues to rigidify after the gel time (as shown in

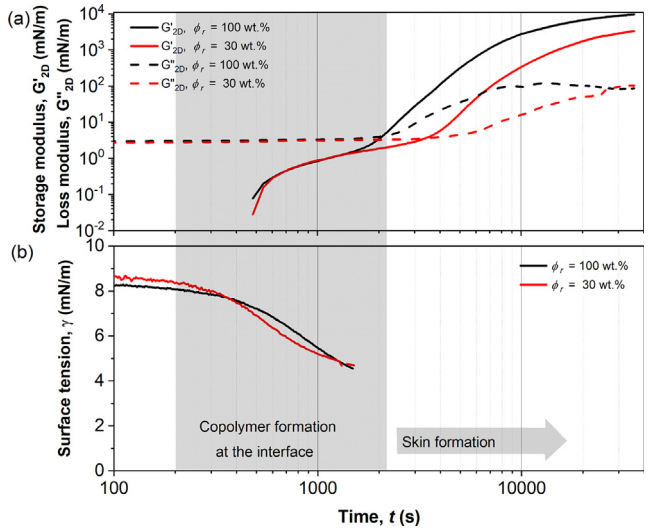

Fig. 7. Characterisation of the temporal evolution of the mechanical properties of the PEG-silicone interface using (a) interfacial shear rheology and (b) pendant drop tensiometry for two different formulations ($\phi_r = 30$ wt.%, 100 wt.% with $\phi_{cat} = 0.3$ vol.%.).

Fig. 5). Further evidence of this skin growth will be provided in Section 3.3. It needs to be noted that the quantitative interpretation of the evolution of the viscoelastic moduli in the limit of long times needs to be treated with care, since the moduli are obtained with the hypothesis of a two-dimensional interface. Beyond 10 000 s the skin thickness approaches values of several 100 μm, making the correctness of this assumption questionable.

3.2. Interfacial tension

To confirm the hypothesis of the copolymer creation given in Section 3.1.2, we carried out surface tension measurements (Section 2.4). The results are shown in Fig. 7b for the same formulations investigated in Fig. 7a ($\phi_r = 30$ wt.% and 100 wt.%, $\phi_{cat} = 0.3$ vol.%). Surface tension starts between 8 and 9 mN/m, which is known for PEG/PDMS interfaces [39]. After about 200 s, the surface tension of both formulations starts to decrease in a similar manner, reaching values around 4.5 mN/m in 1500 s. This decrease can be associated with the formation of PEG-PDMS copolymers due to the Pt-catalysed side-reaction between the OH groups of the PEG and the Si-H groups of the MHDS (reaction A given in Fig. 3). This has also been put in evidence by Giustiniani et al. [39] for a similar system. The surface tension continues to decrease slightly beyond this point; however, the elastic features of the surface of the drop start to play a non-negligible role (confirmed also by the interfacial rheology in Fig. 7a), making the surface tension measurement by shape analysis erroneous [63]. For this reason, we limit the display of the values of interfacial tension to 1500 s only.

Comparing the surface tension measurements with the shear interfacial rheology measurements in Fig. 7a, one observes that the reduction of the surface tension is associated with the first zone where the storage modulus $G\prime_{2D}$ starts to be measurable, indicating that a certain level of elasticity is associated with the presence of the PEG-PDMS copolymers. Considering that the PEG has two OH groups, it may actually act as a cross-linker of the MHDS in the vicinity of the interface, creating therefore a cross-linked network with non-negligible elasticity. Interestingly, during this first step, the evolution of the surface tension and the interfacial elasticity seem fairly independent of the reactive concentration. Future work needs to investigate the influence of ϕ_{cat} and the nature of the PEG-PDMS network to elucidate if it is essentially a dense layer of adsorbed copolymer or a network of crosslinked polymers.

3.3. Skin growth kinetics

We use simple diffusion experiments on flat surfaces and individual drops (as described in Section 2.5) to quantify the thickness evolution of the silicone skin. In both setups, the reaction is allowed to progresses for a given time τ_r before we stop it, either by removing the grid from the silicone blend (in the case of the flat surfaces shown in Fig. 4.I) or by immersing the drops into an inhibitor-filled PDMS blend. The thickness of skins grown on a grid are measured by taking side images using X-ray tomography (Section 2.7). An example of an image obtained with this procedure is shown in Fig. 4.II. The obtained results are shown in Fig. 8.

Since the skin formation is intrinsically linked to the diffusion of the catalyst, the configuration geometry can largely impact the kinetics. We therefore also conduct measurements on individual droploons, as described in Section 2.7. An example of a cryo-SEM image for the formulation $\phi_r = 50.2$ wt.%, $\phi_{cat} = 1.0$ vol.%, $\tau_r = 20$ min is shown in Fig. 2d. The image shows two distinct materials, with the first one forming a (broken) shell around the second. For this formulation and reaction time, we find an average skin thickness of $h_0 = (88 \pm 5)\,\mu$m. The different thickness measurement are summarised in Fig. 8. Despite the small number of data points, one notices that both measurement techniques produce similar results. We hypothesise that the thickness evolution is dominated by the catalyst diffusion and hence to first order independent of the formulation. It can be seen that the skin growth dynamics follows roughly a power law with an exponent of 3/4. Interestingly, if we allow ourselves to draw conclusions from only few data points, the kinetics of skin growth is faster than a diffusive process ($h_0 \propto t^{1/2}$) but slower than ballistic process ($h_0 \propto t$). This may highlight the difference between the skin formation and a simple diffusion process [64–66]. However, the precise mechanism behind the gelation kinetics requires more in-depth investigations.

3.4. Production of emulsions with a millifluidic device

Investigating the effect of interfacial elasticity on the emulsions requires to control the drop size and the reaction time τ_r of each individual droploon. For these reasons, we developed the millifluidic device

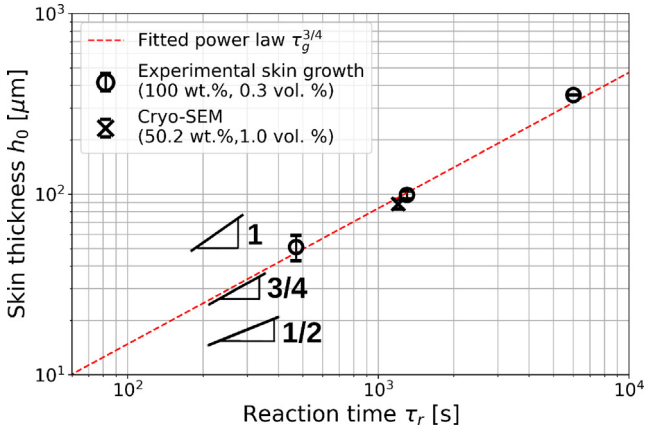

Fig. 8. Skin thickness after different reaction times τ_r for the formulation $\phi_r = 100$ wt.%, $\phi_{cat} = 0.3$ vol.%. Values are obtained for skins grown on a flat interface and imaged with tomography (circles). We add the value obtained with cryo-SEM (cross) for a different formulation of with $\phi_r = 50.2$ wt.%, $\phi_{cat} = 1.0$ vol.%. Symbols represent the average thickness measured at different positions of the skin, while errorbars represent the standard deviation over these measures.

idic setup described in detail in Section 2.6. It provides explicit control over all key parametres: (1) The formulation is set by the concentration of the reactants and their respective flow rates in the circuit. (2) The drop volume is controlled by the flow rates of the dispersed and continuous phase. (3) The skin formation is controlled by allowing the drops to travel for a given reaction time τ_r in the reactive silicone phase in the reaction chamber where the skin can form at the interface, before adding dimethyl maleate in excess concentration to quickly stop the skin formation.

Using this setup, we produce macroscopic monodisperse emulsions of around a thousand identical droploons, controlling ϕ_r, ϕ_{cat} and τ_r separately. An example of an emulsion is shown in Fig. 2e. The variation of the thickness h_0 and rigidity G' of the skin allows to probe the transition from purely capillary to purely elastic interface, i.e. by tuning the elastocapillary number $\alpha = 3G'h_0/\gamma$. The production of droploons with similar elastocapillary number can then be used to investigate the impact of these interfaces on the emulsion morphology. The morphology of these emulsions is investigated using computer-assisted X-ray tomography, with the setup and procedure described in Section 2.7. After algorithmic reconstruction, the image of the sample is saved as stacks of 2D horizontal slices. The images of four samples are shown in Fig. 9, with increasing ϕ_r, ϕ_{cat} and τ_r and capillary number α. The impact of the three parameters still needs to be investigated more systematically to link unequivoqually the parameters of emulsion preparation to the final elastocapillary number of the droploons. However, the four samples shown in Fig. 9 provide some first insight.

A first glance at the images shows already that with the same chemistry but different formulations and reaction times, one has access to a wide range of emulsion structures. The first emulsion in Fig. 9a for low reactive fractions ϕ_r and reaction times τ_r displays a morphology close to an ordinary emulsion at the "jamming" transition where spherical droplets are closely packed without strong deformation [19,1]. With increasing ϕ_r and τ_r one observes that the droploons deform more strongly, i.e., they become more closely packed (Fig. 9b). With even higher ϕ_r and τ_r, the emulsion is composed of mostly interfaces, which become even buckled (Fig. 9c). For the highest ϕ_r and τ_r in Fig. 9d, the droploons behave like packings of capsules, which buckle in their contact zones [35,21,36,37].

We associate this variation in shape and structure to the two-step formation of the silicone skin at the interface. As discussed in Sections 3.1.2 and 3.2, in the first step of the reaction, the copolymers formed at the interface decrease the interfacial tension without increasing significantly the interfacial elasticity of the skin, as shown in Fig. 7. This drop in interfacial tension is seen when comparing Fig. 9a,b, where the packing fraction increases but the drop shapes remain close to the ones in ordinary emulsions, whose deformation is driven purely by interfacial tension effects. Hence, the emulsions a and b correspond to negligibly small elastocapillary numbers α. In the second step of the reaction, the interface crosslinks into a solid-like gel, adding an elastic component to its mechanical response. This is observable by the buckled interfaces, visible in Fig. 9c. As the skin formation progresses, the thickness and rigidity of the skin increases, leading to a skin which is too rigid to stretch upon deformation, but which buckles instead. In this regime, which corresponds to large elastocapillary numbers α, interfacial tension becomes negligible and the droploon shapes are fully dominated by the elastic properties of the droploon shell, i.e., they behave like capsules [35,21,36,37].

The morphology of the emulsions is thus significantly affected by the formation of the skin. While this transition from an emulsion-like structure to buckled shapes can be imagined in the general picture, a separate variation of the different formulation/process parametres is required together with an explicit characterisation of the elastocapillary numbers of these drops. This characterisation could be achieved with pendant drop elastometry [67,63,68,34]. Secondly, it will be important to compare the obtained structures to a predictive model describing their transition from ordinary emulsions to droploon emulsions to capsule packings. A characterisation of the evolution of the emulsion structure with the elastocapillary number α could be investigated using the reconstruction of force and contact networks and the shape of the drops, as proposed in the paper by Roland et al.[1] [69]. As an example, a reconstruction of the sample presented in Fig. 9a is shown in Fig. 9e,f, where red lines represent contact relations between the drops. These emulsions were reconstructed and visualised in 3D with a home-designed segmentation algorithm [70], aimed at the reconstruction of foams and emulsions. The contacts are detected in a physically relevant manner by measuring the distances between interfaces. An example of a reconstruction is shown in Fig. 9e, with the contacts between drops represented with red lines joining the centroids of touching droploons. A vertical view of some droploons of the same sample is shown in Fig. 9f, for a better visualisation of the contact relations.

4. Conclusions and outlook

In this article, we describe and characterise a new experimental model system to investigate the impact of interfacial elastocapillarity on the structure of emulsions. Our system consists of millimetric PEG drops dispersed in a reactive silicone blend, with a catalyst diffusing from the PEG phase to the silicone phase, hence catalysing the crosslinking of a progressively growing layer of silicone gel at the interface. We show that the formation of this skin arises in two steps: we assign the first step to the formation of PEG-PDMS copolymers at the interface, and the second one to the formation of a crosslinked silicone skin of growing thickness. Future investigations will have to reveal the precise nature of the potentially cross-linked copolymer network and its influence on the viscoelastic properties of the overall interface.

We use a dimethyl maleate inhibitor to stop the skin formation, giving it a finite thickness which depends on the formulation and the reaction time. We show that the shear modulus and the gelation kinetics can be controlled separately, allowing to vary skin thickness and rigidity separately to tune the elastocapillary number of the droploons. We further used interfacial shear rheology and different skin thickness measurement techniques to understand better the skin formation and to guide the choice of emulsion production parameters.

Using a millifluidic setup, we produced emulsions of different elastocapillary numbers and showed with tomographic images that a wide range of emulsion morphologies can be obtained from classic emulsions (negligible elastocapillary number) to buckled capsule packings (large elastocapillary number). The accessibility of such a wide range of elastocapillary numbers allows us to go well beyond the preliminary investigations proposed by Giustiniani et al. [39,22] which lacked explicit control over the mechanics of the interface. The system proposed here extends the work by Jose et al. [21,37], who explored the morphology of capsule packings in the elasticity-dominated regime. Future work requires a more systematic variation of the elastocapillary number to separate the effects of the different control parametres (G', h_0 and γ) and to establish quantitative structure/property relations. Within these investigations it will be particularly interesting to explore the properties of systems of $\alpha \approx 0.5$, where capillary and elasticity play on equal footing [34].

[1] in preparation

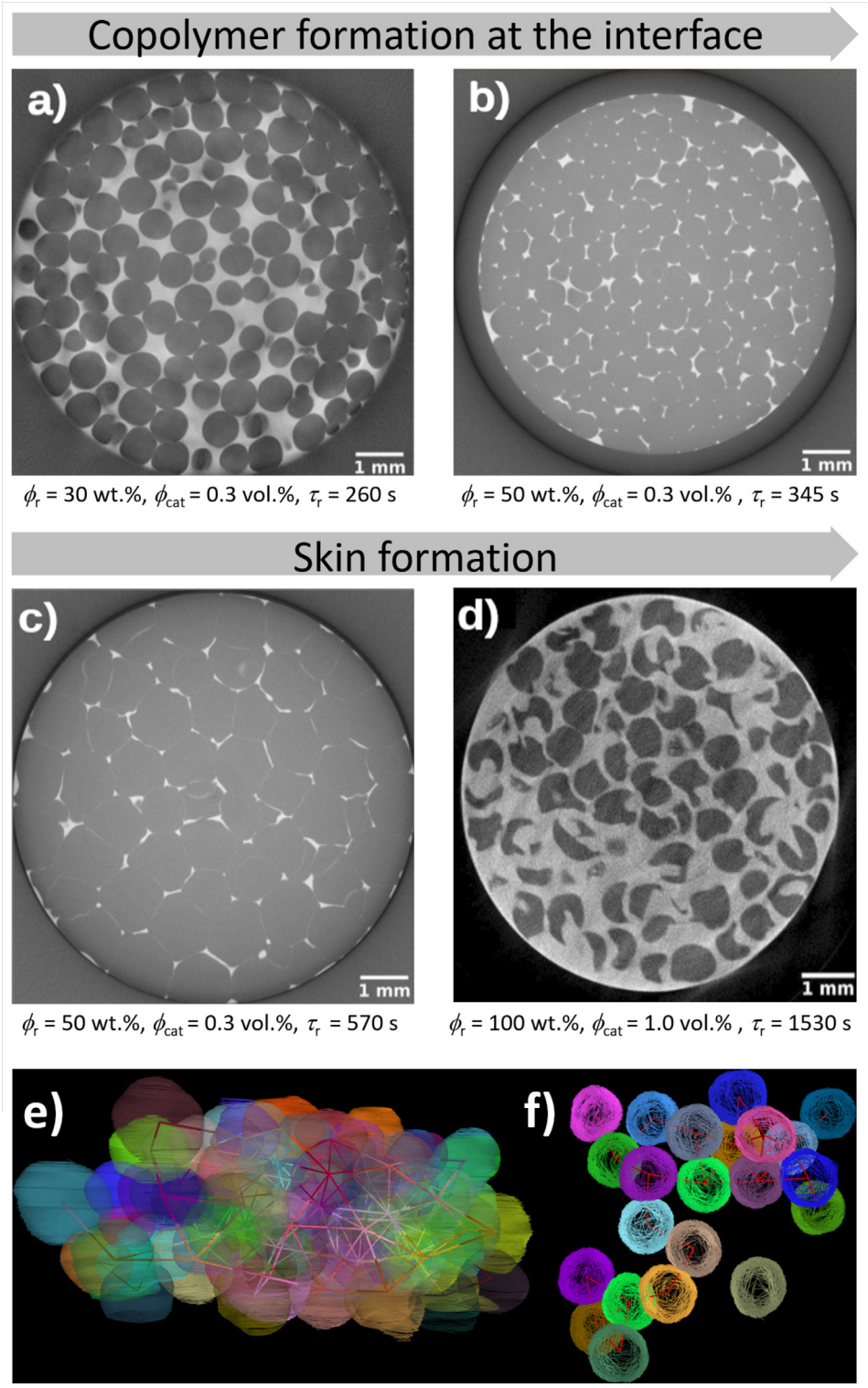

Fig. 9. (a-d) Horizontal slices of emulsions obtained with X-ray tomography with different experimental parameters ($\phi_r, \phi_{cat}, \tau_r$) with decreasing surface tension due to copolymer formation (a → b) and growing importance of the interface elasticity from skin formation (b → c → d). (e,f) 3D reconstruction of the sample shown in (a). (e) When droploons, represented in transparency, are detected as touching at their interface, their contact is represented by a red line joining their centroids. (f) Top view of the same emulsion, reduced to a few droploons. Non-touching droploons, even when really close to each other, are not detected as in contact because of the surface-to-surface distance computation.

Elastocapillary drops and emulsions have been explored in the past, often in the search for "ultra-stable" systems. In this case, solid-like interfacial elasticities are, for example, created by the cross-linking of surfactants, by polyelectrolyte multilayers, by interfacially active particles or by proteines [13,21,57,60,71]. However, these tend to be limited to thin and fragile interfacial layers and to have a narrow range in elastic properties. Our approach goes beyond the state of the art in creating mechanically stable interfaces which allow to span a vast range of elastocapillary numbers - and hence to go from capillary-dominated systems all the way to elasticity-dominated systems with the same chemical formulation. Moreover, by controlling the skin elasticity and the skin thickness

separately, one can tune explicitly the ratio of elastic bending to stretch energy of the interface, which plays a capital role in fixing the response of the interface to deformation and hence the final droploon shape [72].

Further characterisation/optimisation of this system is required before making it a perfectly controlled model system. For example, more advanced mechanical characterisation will be required including dilational [34,60] and large-amplitude deformations. Moreover, future investigations need to explore in depth the influence of the molecular architecture and relative concentrations of the reactive polymers on the skin growth dynamics. As the evolution of the interfacial silicone gel is a complex interplay of chemical kinetics and hindered spatial diffusion, an exhaustive understanding of its formation is required to know the advancement of the gelation at different times and points of the skin. Similar investigations have been proposed for skins formed by electrostatic or hydrogen bonding [66,65], but they still await to be exploited to control emulsion morphologies.

Since our approach can be used with different dispersed liquids (provided that they are immiscible with silicone), we believe that it will provide important inspiration for the generation of silicone polyHIPES (polymerised High Internal Phase Emulsions) in terms of formulation and morphology control. The interest in silicone polyHIPES is rapidly growing [3,73–75], due to their outstanding chemical/mechanical/optical properties of importance for a wide range of applications from water purification via adhesion control to tissue engineering.

Last but not least, while we concentrated on using the droploons as elements composing emulsions, the same approach is equally interesting for the direct generation of individual silicone capsules of controlled size and mechanical properties. In contrast to previously used methods [76,77], our approach allows to combine capsule fabrication and filling within one single microfluid chip while providing access to a wide range of capsule shells thicknesses down to sub-micron thicknesses.

Declaration of Competing Interest

The authors declare that they have no known competing financial interests or personal relationships that could have appeared to influence the work reported in this paper.

Acknowledgements

The authors would like to thank Anaïs Giustiniani, Christophe Poulard, Aurélie Hourlier-Fargette and François Ganachaud for in-depth discussions. We thank Matthias Schröter for precious help with the tomographic analysis and Elkem Silicones for useful informations and the provision of the non-reactive silicones. This work has been financed by an ERC Consolidator Grant (agreement 819511 – METAFOAM) and profited also from an IdEx Unistra "Attractivity grant" (Chaire W. Drenckhan). It was conducted in the framework of the Interdisciplinary Institute HiFunMat, as part of the ITI 2021–2028 program of the University of Strasbourg, CNRS and Inserm, was supported by IdEx Unistra (ANR-10-IDEX-0002) and SFRI (STRATUS project, ANR-20-SFRI-0012) under the framework of the French Investments for the Future Program. The authors acknowledge the CarMac and Plamics facilities of ICS for the use of the SEC, the ATG and the cryo-SEM microscope.

Appendix A. Supplementary data

Supplementary data to this article can be found online at https://doi.org/10.1016/j.jcis.2022.07.029.

References

[1] W. Drenckhan, S. Hutzler, Structure and energy of liquid foams, Adv. Colloid Interface Sci. 224 (2015) 1–16, https://doi.org/10.1016/j.cis.2015.05.004. URL http://www.sciencedirect.com/science/article/pii/S0001868615000858.
[2] D. Weaire, S. Hutzler, Physics of foams, Oxford University Press, 1999.
[3] K.A.T. Silverstein, Emulsion-templated polymers: Contemporary contemplations, Polymer 126 (2017) 261–282.
[4] S.D. Kimmins, N.R. Cameron, Functional Porous Polymers by Emulsion Templating: Recent Advances, Adv. Funct. Mater. 21 (2) (2011) 211–225, https://doi.org/10.1002/adfm.201001330.
[5] S. Andrieux, A. Quell, C. Stubenrauch, W. Drenckhan, Liquid foam templating - A route to tailor-made polymer foams, Adv. Colloid Interface Sci. 256 (2018) 276–290, https://doi.org/10.1016/j.cis.2018.03.010. URL http://www.sciencedirect.com/science/article/pii/S0001868618300216.
[6] C. Stubenrauch, A. Menner, A. Bismarck, W. Drenckhan, Emulsion and Foam Templating-Promising Routes to Tailor-Made Porous Polymers, Angew. Chem. Int. Ed. 57 (32) (2018) 10024–10032, https://doi.org/10.1002/anie.201801466.
[7] M. Ashby, The properties of foams and lattices, Philosophical Transactions of the Royal Society A: Mathematical, Physical and Engineering Sciences 364 (1838) (2006) 15–30, https://doi.org/10.1098/rsta.2005.1678. URL https://royalsocietypublishing.org/.
[8] X. Zheng, H. Lee, T. Weisgraber, M. Shusteff, J. DeOtte, E. Duoss, J. Kuntz, M. Biener, Q. Ge, J. Jackson, S. Kucheyev, N. Fang, C. Spadaccini, Ultralight, ultrastiff mechanical metamaterials, Science 344 (6190) (2014) 1373–1377, https://doi.org/10.1126/science.1252291.
[9] R. Gatt, L. Mizzi, J. Azzopardi, K. Azzopardi, D. Attard, A. Casha, J. Briffa, J. Grima, Hierarchical Auxetic Mechanical Metamaterials 5 (2015) 8395, https://doi.org/10.1038/srep08395.
[10] H. Kolken, A. Zadpoor, Auxetic mechanical metamaterials, RSC Advances 7 (9) (2017) 5111–5129, https://doi.org/10.1039/C6RA27333E.
[11] D.R. Reid, N. Pashine, J.M. Wozniak, H. Jaeger, A. Liu, S. Nagel, J. de Pablo, Auxetic metamaterials from disordered networks, Proceedings of the National Academy of Sciences 115 (7) (2018) E1384 LP – E1390. doi:10.1073/pnas.1717442115. http://www.pnas.org/content/115/7/E1384.abstract.
[12] M. Porter, N. Ravikumar, F. Barthelat, R. Martini, 3d-printing and mechanics of bio-inspired articulated and multi-material structures, Journal of the mechanical behavior of biomedical materials 73 (2017) 114–126.
[13] C.P. Whitby, L. Lotte, C. Lang, Structure of concentrated oil-in-water Pickering emulsions, Soft Matter 8 (30) (2012) 7784–7789, https://doi.org/10.1039/C2SM26014J.
[14] F. Graner, D. Riveline, 'The Forms of Tissues, or Cell-aggregates': D'Arcy Thompson's influence and its limits, Development 144 (23) (2017) 4226–4237, https://doi.org/10.1242/dev.151233. URL http://dev.biologists.org/content/develop/144/23/4226.full.pdf.
[15] A. Alcinesio, O.J. Meacock, R.G. Allan, C. Monico, V. Restrepo Schild, I. Cazimoglu, M.T. Cornall, R. Krishna Kumar, H. Bayley, Controlled packing and single-droplet resolution of 3D-printed functional synthetic tissues, Nature, Communications 11 (1) (2020) 2105, https://doi.org/10.1038/s41467-020-15953-y.
[16] M.M. Makhoul-Mansour, E.C. Freeman, Droplet-Based Membranous Soft Materials, Langmuir 37 (11) (2021) 3231–3247, https://doi.org/10.1021/acs.langmuir.0c03289.
[17] C. O'Hern, L. Silbert, A. Liu, S. Nagel, Jamming at zero temperature and zero applied stress: The epitome of disorder, Physical Review E - Statistical Physics, Plasmas, Fluids, and Related Interdisciplinary Topics 68 (1) (2003) 19. arXiv:0304421, doi:10.1103/PhysRevE.68.011306.
[18] A. Siemens, M. Van Hecke, Jamming: A simple introduction, Phys. A 389 (20) (2010) 4255–4264, https://doi.org/10.1016/j.physa.2010.02.027.
[19] M. Van Hecke, Jamming of soft particles: Geometry, mechanics, scaling and isostaticity, Journal of Physics Condensed Matter 22 (3) (2010), https://doi.org/10.1088/0953-8984/22/3/033101. arXiv:0911.1384.
[20] A. Pogorelov, Bendings of surfaces and stability of shells, American Mathematical Soc. 72 (1988).
[21] J. Jose, G.A. Blab, A. Van Blaaderen, A. Imhof, Jammed elastic shells-a 3d experimental soft frictionless granular system, Soft Matter 11 (9) (2015) 1800–1813, https://doi.org/10.1039/C4SM02098G.
[22] A. Giustiniani, S. Weis, C. Poulard, P. Kamm, F. Garcia-Moreno, M. Schroter, W. Drenckhan, Skinny emulsions take on granular matter, Soft Matter 14 (36) (2018) 7310–7323, https://doi.org/10.1039/c8sm00830b.
[23] R. Höhler, Y. Sang, E. Lorenceau, S. Cohen-Addad, Osmotic Pressure and Structures of Monodisperse Ordered Foam, Langmuir 24 (2) (2007) 418–425.
[24] S. Andrieux, W. Drenckhan, C. Stubenrauch, Highly ordered biobased scaffolds: From liquid to solid foams, Polymer 126 (Supplement C) (2017) 425–431, https://doi.org/10.1016/j.polymer.2017.04.031. URL http://www.sciencedirect.com/science/article/pii/S0032386117303993.
[25] A. Testouri, C. Honorez, A. Barillec, D. Langevin, W. Drenckhan, Highly Structured Foams from Chitosan Gels, Macromolecules 43 (14) (2010) 6166–6173.
[26] A. Testouri, Highly structured polymer foams from liquid foam templates using millifluidic lab-on-a-chip techniques, Ph.D. thesis (2012).
[27] A. Giustiniani, W. Drenckhan, Linking Adhesive Properties and Pore Organisation of Silicone Emulsions Obtained by Reactive Blending, Ph.D. thesis (2017).
[28] L. Arriaga, W. Drenckhan, A. Salonen, J. Rodrigues, R. Iniguez-Palomares, E. Rio, D. Langevin, On the long-term stability of foams stabilised by mixtures of

nano-particles and oppositely charged short chain surfactants, Soft Matter 8 (43) (2012) 11085–11097, https://doi.org/10.1039/c2sm26461g.
[29] A. van der Net, A. Gryson, M. Ranft, F. Elias, C. Stubenrauch, W. Drenckhan, Highly structured porous solids from liquid foam templates, Colloids Surf., A 346 (1–3) (2009) 5–10.
[30] A. Testouri, L. Arriaga, C. Honorez, M. Ranft, J. Rodrigues, A. van der Net, A. Lecchi, A. Salonen, E. Rio, R. Guillermic, D. Langevin, W. Drenckhan, Generation of porous solids with well-controlled morphologies by combining foaming and flow chemistry on a Lab-on-a-Chip, Colloids and Surfaces a-Physicochemical and Engineering Aspects 413 (2012) 17–24, https://doi.org/10.1016/j.colsurfa.2012.02.048.
[31] A. Quell, S. Heitkam, W. Drenckhan, C. Stubenrauch, Creating Honeycomb Structures in Porous Polymers by Osmotic Transport, Chemphyschem 18 (5) (2017) 451–454, https://doi.org/10.1002/cphc.201600834.
[32] M. Llorente, J. Mark, Model networks of end-linked poly (dimethylsiloxane) chains. 8. networks having cross-links of very high functionality, Macromolecules 13 (3) (1980) 681–685.
[33] F. Chambon, H. Winter, Linear viscoelasticity at the gel point of a crosslinking pdms with imbalanced stoichiometry, J. Rheol. 31 (8) (1987) 683–697.
[34] G. Ginot, F.S. Kratz, F. Walzel, J. Farago, J. Kierfeld, R. Höhler, W. Drenckhan, Pressure-deformation relations of elasto-capillary drops (droploons) on capillaries, Soft Matter 17 (40) (2021) 9131–9153.
[35] C.I. Zoldesi, I.L. Ivanovska, C. Quilliet, G.J. Wuite, A. Imhof, L. Pauchard, S. Rica, C.I. Zoldesi, I.L. Ivanovska, C. Quilliet, G.J. Wuite, A. Imhof, Elastic properties of hollow colloidal particles, Physical Review E - Statistical, Nonlinear, and Soft Matter Physics 78 (5) (1998) 1–8, https://doi.org/10.1103/PhysRevE.78.051401.
[36] C. Quilliet, C. Zoldesi, C. Riera, A. Van Blaaderen, A. Imhof, Anisotropic colloids through non-trivial buckling, Eur. Phys. J. E 27 (2008) 13–20, https://doi.org/10.1140/epje/i2007-10365-2.
[37] J. Jose, A. Van Blaaderen, A. Imhof, Random three-dimensional jammed packings of elastic shells acting as force sensors, Phys. Rev. E 93 (6) (2016) 1–14, https://doi.org/10.1103/PhysRevE.93.062901.
[38] L. Lewis, J. Stein, R. Colborn, Y. Gao, J. Dong, The chemistry of fumarate and maleate inhibitors with platinum hydrosilylation catalysts, J. Organomet. Chem. 521 (1–2) (1996) 221–227, https://doi.org/10.1016/0022-328X(96)06247-X.
[39] A. Giustiniani, P. Guégan, M. Marchand, C. Poulard, W. Drenckhan, Generation of Silicone Poly-HIPEs with Controlled Pore Sizes via Reactive Emulsion Stabilization, Macromol. Rapid Commun. 37 (18) (2016) 1527–1532, https://doi.org/10.1002/marc.201600281.
[40] J. Stein, L. Lewis, K. Smith, K. Lettko, Mechanistic studies of platinum-catalyzed hydrosilylation, J. Inorg. Organomet. Polym. 1 (3) (1991) 325–334.
[41] J. Braun, J. Mark, B. Eichinger, Formation of Poly(dimethylsiloxane) Gels, Macromolecules 35 (7) (2002) 5273–5282, https://doi.org/10.1021/ma0116046.
[42] B. Marciniec, Z. Foltynowicz, M. Lewandowski, Catalysis of hydrosilylation, part xxii: Polymer-protected immobilized platinum complex catalysts for gas-phase hydrosilylation of acetylene, Applied organometallic chemistry 7 (3) (1993) 207–212.
[43] Y. Nakajima, S. Shimada, Hydrosilylation reaction of olefins: recent advances and perspectives, RSC advances 5 (26) (2015) 20603–20616.
[44] A. Chalk, J. Harrod, I.I. Homogeneous Catalysis, The Mechanism of the Hydrosilation of Olefins Catalyzed by Group VIII Metal Complexes, Journal of the American Chemical Society 87(1) (1965) 16–21, https://doi.org/10.1021/ja01079a004.
[45] B. Karstedt, Platinum complexes of unsaturated siloxanes and platinum containing organopolysiloxanes (apr 1971).
[46] L. Lestel, H. Cheradame, S. Boileau, Crosslinking of polyether networks by hydrosilylation and related side reactions, Polymer 31 (6) (1990) 1154–1158.
[47] N. Alcantar, E. Aydil, J. Israelachvili, Polyethylene glycol-coated biocompatible surfaces, J. Biomed. Mater. Res. 51 (3) (2000) 343–351, https://doi.org/10.1002/1097-4636(20000905)51:3<343::AID-JBM7>3.0.CO;2-D.
[48] A. Esteves, J. Brokken-Zijp, J. Laven, H. Huinink, N. Reuvers, M. Van, G. de With, Influence of cross-linker concentration on the cross-linking of PDMS and the network structures formed, Polymer 50 (16) (2009) 3955–3966, https://doi.org/10.1016/j.polymer.2009.06.022.
[49] G.G. Fuller, J. Vermant, Complex Fluid-Fluid Interfaces: Rheology and Structure, Annu. Rev. Chem. Biomol. Eng. 3 (1) (2012) 519–543, https://doi.org/10.1146/annurev-chembioeng-061010-114202.
[50] T. Instruments, Interfacial rheology: accessories (2021). https://www.tainstruments.com/wp-content/uploads/Interfacial-Cell-Spread.pdf.
[51] H. Winter, Can the gel point of a cross-linking polymer be detected by the G' - G crossover?, Polym. Eng. Sci. 27 (22) (1987) 1698–1702, https://doi.org/10.1002/pen.760272209. URL https://doi.org/10.1002/pen.760272209.
[52] K. Suman, Y. Joshi, On the universality of the scaling relations during sol-gel transition, J. Rheol. 64 (4) (2020) 863–877, https://doi.org/10.1122/1.5134115.
[53] D. Alexander, Levenberg-marquardt toolbox, https://www.mathworks.com/matlabcentral/fileexchange/53449-levenberg-marquardt-toolbox (2021).
[54] K. Dušek, W. Prins, Structure and elasticity of non-crystalline polymer networks, in: Fortschritte der Hochpolymeren-Forschung, Springer, Berlin Heidelberg, Berlin, Heidelberg, 1969, pp. 1–102, https://doi.org/10.1007/BFb0051042.
[55] C. Creton, 50th anniversary perspective: Networks and gels: Soft but dynamic and tough, Macromolecules 50 (21) (2017) 8297–8316. arXiv:https://doi.org/10.1021/acs.macromol.7b01698, doi:10.1021/acs.macromol.7b01698. doi:10.1021/acs.macromol.7b01698.
[56] M. Zhong, R. Wang, K. Kawamoto, B.D. Olsen, J.A. Johnson, Quantifying the impact of molecular defects on polymer network elasticity, Science 353 (6305) (2016) 1264–1268. arXiv:https://www.science.org/doi/pdf/10.1126/science.aag0184, doi:10.1126/science.aag0184. https://www.science.org/doi/abs/10.1126/science.aag0184.
[57] H. Rehage, M. Husmann, A. Walter, From two-dimensional model networks to microcapsules, Rheol. Acta 41 (4) (2002) 292–306, https://doi.org/10.1007/s00397-002-0233-3.
[58] L.M.C. Sagis, P. Fischer, Nonlinear rheology of complex fluid-fluid interfaces, Curr. Opin. Colloid Interface Sci. 19 (6) (2014) 520–529, https://doi.org/10.1016/j.cocis.2014.09.003. URL http://www.sciencedirect.com/science/article/pii/S1359029414000909.
[59] N. Jaensson, J. Vermant, Tensiometry and rheology of complex interfaces, Curr. Opin. Colloid Interface Sci. 37 (2018) 136–150, https://doi.org/10.1016/j.cocis.2018.09.005. URL http://www.sciencedirect.com/science/article/pii/S1359029418300062.
[60] M. Pepicelli, N. Jaensson, C. Tregouet, B. Schroyen, A. Alicke, T. Tervoort, C. Monteux, J. Vermant, Surface viscoelasticity in model polymer multilayers: From planar interfaces to rising bubbles, J. Rheol. 63 (2019) 815–828, https://doi.org/10.1122/1.5096887.
[61] A.V. Bayles, J. Vermant, Divide, Conquer, and Stabilize: Engineering Strong Fluid-Fluid Interfaces, Langmuir 38 (21) (2022) 6499–6505, https://doi.org/10.1021/acs.langmuir.2c00948.
[62] A. Giustiniani, W. Drenckhan, C. Poulard, Interfacial tension of reactive, liquid interfaces and its consequences, in: Advances in Colloid and Interface Science 247 (Supplement C), 2017, pp. 185–197, https://doi.org/10.1016/j.cis.2017.07.017.
[63] M. Nagel, T. Tervoort, J. Vermant, From drop-shape analysis to stress-fitting elastometry, Adv. Colloids Interface Sci. 247 (July) (2017) 33–51, https://doi.org/10.1016/j.cis.2017.07.008.
[64] A. Blandino, M. Macías, D. Cantero, Formation of calcium alginate gel capsules: Influence of sodium alginate and CaCl2 concentration on gelation kinetics, J. Biosci. Bioeng. 88 (6) (1999) 686–689, https://doi.org/10.1016/S1389-1723(00)87103-0. URL http://www.sciencedirect.com/science/article/pii/S1389172300871030.
[65] J.D. de Baubigny, P. Perrin, N. Pantoustier, T. Salez, M. Reyssat, C. Monteux, Growth Mechanism of Polymer Membranes Obtained by H-Bonding Across Immiscible Liquid Interfaces, ACS Macro Lett. 10 (2) (2021) 204–209, https://doi.org/10.1021/acsmacrolett.0c00847.
[66] B. Keshavarzi, K. Schwarzenberger, M. Huang, A. Javadi, K. Eckert, Formation of Structured Membranes by Coacervation of Xanthan Gum with CnTAB Surfactants, Langmuir 35 (42) (2019) 13624–13635, https://doi.org/10.1021/acs.langmuir.9b02220.
[67] S. Knoche, D. Vella, E. Aumaitre, P. Degen, H. Rehage, P. Cicuta, J. Kierfeld, Elastometry of Deflated Capsules: Elastic Moduli from Shape and Wrinkle Analysis, Langmuir 29 (40) (2013) 12463–12471, https://doi.org/10.1021/la402322g.
[68] J. Hegemann, S. Knoche, S. Egger, M. Kott, S. Demand, A. Unverfehrt, H. Rehage, J. Kierfeld, Pendant capsule elastometry, J. Colloids Interface Sci. 513 (Supplement C) (2018) 549–565, https://doi.org/10.1016/j.jcis.2017.11.048. URL http://www.sciencedirect.com/science/article/pii/S002197971731353X.
[69] G. Ginot, Interfacially-controlled soft granular matter: from non-pairwise to elastocapillary interactions in foams and emulsions stabilised by polymeric skins, Ph.D. thesis (2017).
[70] G. Ginot, Vritra: a segmentation/reconstruction algorithm for contact detection in foams and emulsions, https://github.com/SimianLibrarian/vritra (2021).
[71] D. Gonzalez Ortiz, C. Pochat-Bohatier, J. Cambedouzou, M. Bechelany, P. Miele, Current Trends in Pickering Emulsions: Particle Morphology and Applications, Engineering 6 (4) (2020) 468–482. doi: 10.1016/j.eng.2019.08.017. https://www.sciencedirect.com/science/article/pii/S2095809919305594.
[72] D.P. Holmes, Elasticity and stability of shape-shifting structures, Curr. Opin. Colloid Interface Sci. 40 (2019) 118–137, https://doi.org/10.1016/j.cocis.2019.02.008. URL https://www.sciencedirect.com/science/article/pii/S1359029418300839.
[73] D.Y. Zhu, S. Handschuh-Wang, X.C. Zhou, Recent progress in fabrication and application of polydimethylsiloxane sponges, J. Mater. Chem. A 5 (32) (2017) 16467–16497, https://doi.org/10.1039/c7ta04577h.
[74] A. Kataruka, S.B. Hutchens, PDMS polymerized high internal phase emulsions (polyHIPEs) with closed-cell, aqueous-filled microcavities, Soft Matter 15 (47) (2019) 9665–9675, https://doi.org/10.1039/C9SM01732A.
[75] P. Mazurek, B.E.F. Ekbrant, F.B. Madsen, L. Yu, A.L. Skov, Glycerol-silicone foams - Tunable 3-phase elastomeric porous materials, Eur. Polym. J. 113 (2019) 107–114, https://doi.org/10.1016/j.eurpolymj.2019.01.051.
[76] C. Vilanova, Neus Rodríguez-Abreu, A. Fernández-Nieves, C. Solans, Fabrication of Novel Silicone Capsules with Tunable Mechanical Properties by Microfluidic Techniques, ACS Applied Materials and Interfaces 5 (11) (2013) 5247–5252. doi:10.1021/am4010896. doi: 10.1021/am4010896.
[77] Z. Fu, L. Su, J. Li, R. Yang, Z. Zhang, M. Liu, J. Li, B. Li, Elastic silicone encapsulation of n-hexadecyl bromide by microfluidic approach as novel microencapsulated phase change materials, Thermochim. Acta 590 (2014) 24–29, https://doi.org/10.1016/j.tca.2014.06.008. URL https://www.sciencedirect.com/science/article/pii/S004060311400269X.